Penerbit UTHM

IJIE

Journal homepage: http://penerbit.uthm.edu.my/ojs/index.php/ijie
ISSN : 2229-838X e-ISSN : 2600-7916

The International Journal of Integrated Engineering

Towards Laparoscopic Visual AI: Development of a Visual Guidance System for Laparoscopic Surgical Palpation

Kerwin G. Caballas[1,2*], Harold Jay M. Bolingot[2], Nathaniel Joseph C. Libatique[3], Gregory L. Tangonan[2]

[1]Department of Information Systems and Computer Science,
Ateneo De Manila University, Quezon City, 1108, PHILIPPINES

[2]Ateneo Innovation Center,
Ateneo De Manila University, Quezon City, 1108, PHILIPPINES

[3]Department of Electronics, Computer, and Communications Engineering,
Ateneo De Manila University, Quezon City, 1108, PHILIPPINES

*Corresponding Author

DOI: https://doi.org/10.30880/ijie.2021.13.05.004
Received 15 April 2021; Accepted 30 April 2021; Available online 31 July 2021

Abstract: Currently, there are numerous obstacles to performing palpation during laparoscopic surgery. The laparoscopic interface does not allow access into a patient's body anything other than the tools that are inserted through the trocars. Palpation is usually done with the surgeon's hands to detect lumps and certain anomalies underneath the skin, muscle, or tissues. It can be useful technique for augmenting surgical decision-making during laparoscopic surgery, especially when discerning operations involving cancerous tumors. Previous research demonstrated the use of tactile sensors and mechanical sensors placed at the end-effectors for palpating laparoscopically. In this study, a visual guidance system is proposed for use during laparoscopic palpation, specifically engineered to be part of a motion-based laparoscopic palpation system. In particular, the YOLACT++ model is used to localize a target organ, the gall bladder, on a custom dataset of laparoscopic cholecystectomy. Our experiments showed an AP score of 90.10 for bounding boxes and 87.20 on masks. In terms of the speed performance, the model achieved a playback speed of approximately 20 fps, which translates to approximately 48 ms video latency. The palpation path guides are guidelines that are computer-generated within the identified organ, and they show potential in helping the surgeon implement the palpation more accurately. Overall, this study demonstrates the potential of deep learning-based real-time image processing models to complete our motion-based laparoscopic palpation system, and to realize the promising role of artificial intelligence in surgical decision-making. Visual presentation of our results can be seen on our project page: https://kerwincaballas.github.io/lap-palpation.

Keywords: Laparoscopic palpation, surgical computer vision, instance segmentation, image-guided surgery, artificial intelligence, surgical decision-making.

1. Introduction

Palpation is one of the more common techniques being used when detecting tissue anomalies. During palpation, haptic information about the tissue being palpated can be obtained, such as its size, shape, and texture. Palpation is relatively easier and relatively faster to perform compared to other anomaly detection techniques, only needing the surgeons to examine the tissue for anomalies. In this process, haptic information is used to physically determine the

*Corresponding author: kerwin.caballas@obf.ateneo.edu

location and presence of lumps, such as stones, cysts, tumors, or other types of mass. Palpation is generally used to physically determine the location and presence of lumps, such as stones, cysts, tumors, or other types of mass.

Palpation is not an issue during open surgery since surgeons can easily perform palpation directly on the patient's body. However, it is almost impossible to perform this during laparoscopic surgery, when surgeons cannot access the patient's viscera using their hands. Previous work by the authors have tackled this problem by developing a motion-based intraoperative laparoscopic palpation system [1]. The system made use of a wearable motion-sensing armband which measured the acceleration of the arm when worn.

In this study, we propose a visual guidance subsystem to assist our previously developed motion-based laparoscopic palpation system. Our visual guidance subsystem is based on a computer vision technique called instance segmentation, that can accurately detect tissues and organs of interest during laparoscopic surgery. Specifically, the objective of this study is to develop the visual guidance component of the motion-based laparoscopic palpation system based on a real-time instance segmentation computer vision model. The functions of the visual guidance component are as follows: (1) highlight a specific organ while on view, and (2) generate a computer-generated image path guides as a visual assistance for the laparoscopic palpation action.

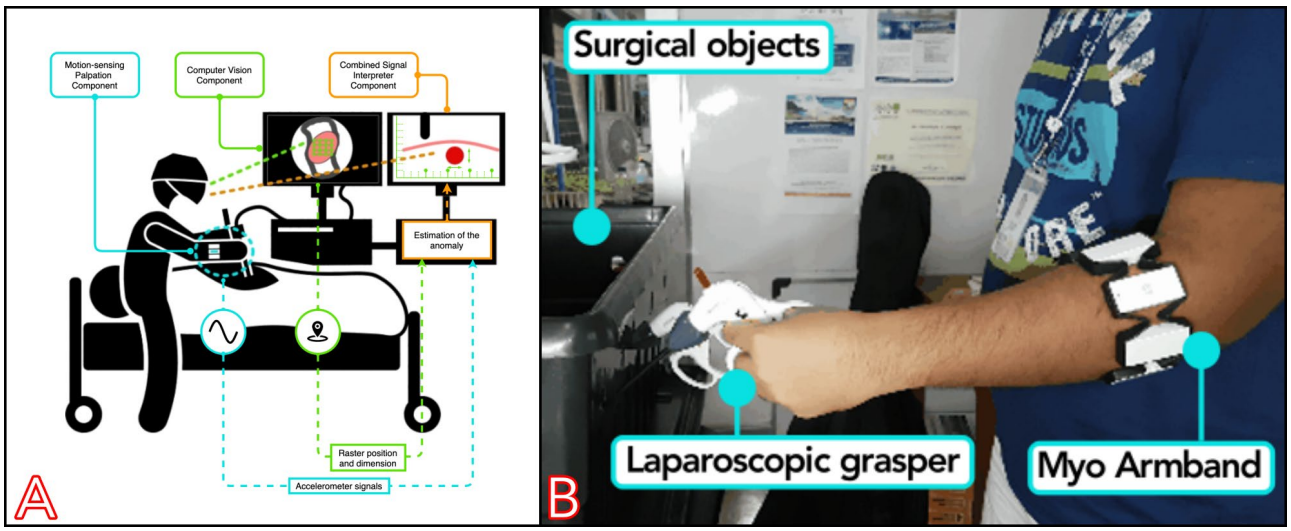

Fig. 1 - (A) System diagram of the entire motion-sensing laparoscopic palpation system. The motion-sensing palpation component is denoted in blue lines. The visual guidance component is denoted in green lines. The combined signal interpreter component is denoted in orange lines; (B) Motion-based intraoperative laparoscopic palpation system previously developed by the authors which detected anomalies through prodding target areas with a laparoscopic grasper. The system used a wearable motion-sensing armband (Myo Armband) to detect changes in the acceleration of the arm [1]

As shown in Fig. 1, our overall motion-based laparoscopic palpation system allows the surgeon to palpate on a target tissue or organ, laparoscopically, using the Myo Armband gesture controller, and infer the structure of the anomaly being detected based on the output data that the system will generate. There are three components in this overall motion-based laparoscopic palpation system. The first system is the motion-sensing palpation component. This system consists of the Myo Armband gesture controller [2], a wearable motion-sensing armband which has an accelerometer that can measure the 3-axis acceleration (in units of g) of the arm when worn. In addition to the accelerometer, the Myo Armband also has eight surface-based EMG electrodes that wirelessly streams surface-based electromyography signals at 200-Hz sampling rate [3]. This signal has been used to ergonomically analyze the different gestures of using a commercial laparoscopic tool, which thus shows that the Myo Armband gesture controller has a wide range of functions in analyzing and improving laparoscopic surgical performance [3].

Fig. 2 shows the accelerometer waveform that is being recorded and analyzed in this component. For this component to work, the surgeon will prod the area of tissue to be examined using a laparoscopic tool as the surgeon wears the motion-sensing armband. As demonstrated in [1], the armband measures the acceleration of the prodding arm, detecting changes as the end-effector of the tool being used collided with the surface of the tissue model. The tissue model contains an embedded anomaly that protrudes the top layer of the model. Due to this protrusion, the series of prodding the physical markers eventually reaches a scenario when the altitude gap between the end-effector mid-air and the surface of the tissue model decreases. This system is then able to infer the presence and position of the embedded anomaly by calculating the average peak-to-peak amplitude of the recorded acceleration signal. The decrease in the average peak-to-peak amplitude of the acceleration denotes reaching the area of protrusion in the tissue model, which in turn indicates the position of the anomaly. In terms of kinematics, this decrease is due to the lesser time for the

end-effector to accelerate towards the surface of the tissue model, with the altitude gap between the end-effector and the surface of the tissue model decreasing due to the protrusion on the tissue model by the embedded anomaly. It was demonstrated that prodding an artificial tissue model with the end-effector can detect an embedded anomaly for up to 2 cm [1].

The second component of our motion-sensing laparoscopic palpation system is the visual guidance component, which is the idea behind this paper. The function of the visual guidance component is to visually assist the surgeon in the series of prodding, by visualizing the prodding points in the target organ onto the monitor that is streaming the laparoscope image, in a feature we will call 'palpation path guides.' This feature is equivalent to the physical markers on the artificial tissue model in Fig. 2.c. The third component is the combined signal interpreter component. This component receives the accelerometer signal from the first component, as well as the corresponding location and measurement data from the second component, processes these signals, and generates an estimation of the anomaly to the surgeon, in a separate monitor from the laparoscope images. This component is being planned for development in the future.

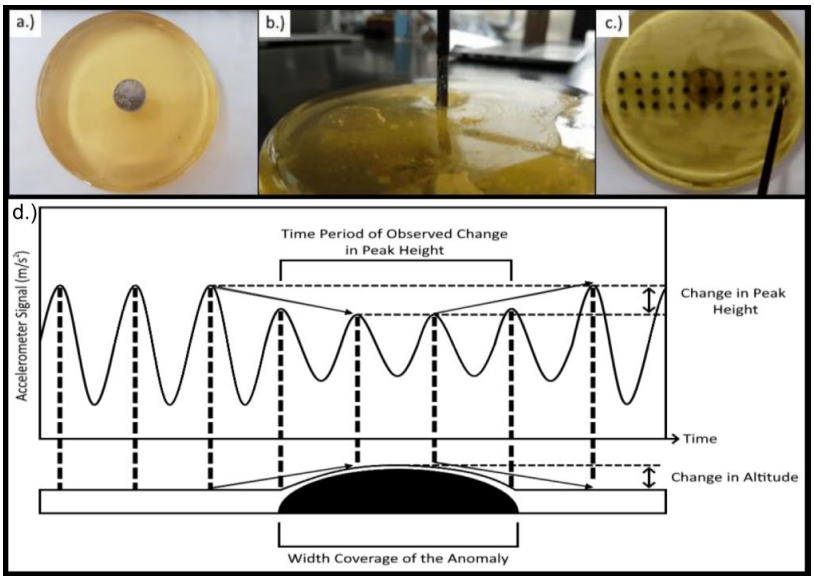

Fig. 2 - Top-row: (a) artificial tissue model with embedded anomaly; (b) prodding of the end-effector on the tissue model; (c) physical markers for prodding on the tissue model [1]. Bottom-row; (d) visualization of the accelerometer waveform and the position and dimension of the embedded anomaly in the artificial tissue model [1]

2. Related Literature

2.1 Palpation in Laparoscopic Surgery

Palpation is the medical procedure for finding out internal abnormalities by using hands [4]. During surgery, the palpating surgeon must be able to measure tissue properties and feel their variations [5]. Palpation in surgery is sometimes done because visual or imaging inspection alone may not be able to properly detect tumors, nerves, vessels, and other hard organic structures buried under the tissue surface [6]. This is where the sense of touch might prove to be more valuable. The standard magnetic resonance imaging (MRI) technique cannot always properly determine the presence and location of tumors that are less than 1 cm in diameter [7-9]. One of the reasons why radiological imaging techniques such as MRI and ultrasound are problematic in this scenario is due to poorer image contrast and spatial resolutions [10, 11]. In cases where such radiological imaging techniques cannot provide clearer views of tissue lesions, palpation can be utilized by the surgeon to add another tool of perception for extracting more information such as the locations and dimensions of those lesions [10]. Over the past several years, innovations have been introduced to augment minimally invasive surgical techniques, including laparoscopy, endoscopy, and robot-assisted surgery. The integration of artificial intelligence, robotics, and sensors brought about significant developments in laparoscopic surgery. Different techniques have been proposed to introduce the sense of touch into the laparoscopic interface, such as force-sensing [5], [12-13]. Innovations such as integrating sensors into the laparoscopic tools have also emerged, like force-sensitive forceps [15-17], sensor-enforced graspers [13], and sensor-integrated scalpels [18-19].

2.2 Computer Vision in Surgery

Visually, localization is challenging in laparoscopic surgery because the surgeon's field of view is limited to the anatomical surface directly in front of the endoscope [20]. The application of computer vision provides a path towards augmenting the experience of laparoscopic surgery by providing the critical information to the surgeon from the 3D shape of tissue surfaces and corresponding morphology from the endoscopic images streaming from the camera. This has been the goals of image-guided surgery [21-23]. Endoscopic and laparoscopic surgery have essentially brought a digital camera to the operating room [23]. The recorded laparoscopic images provide a wealth of information, yet substantially underused, as processing this amount of information in real time is very challenging and computationally expensive, for computers and for humans. However, the increased computational capabilities and recent advances in machine learning and data science now provide a path for computer systems to understand the content of an image or a video stream in real time, and thereby augment the surgeon. In this regard, deep learning has been demonstrated to perform detection of tissues, organs, and instruments in an endoscope video dataset of laparoscopic hysterectomies, using an instance segmentation method. The deep learning model used was Mask-RCNN, a popular model for instance segmentation, that can highlight the irregularly shaped object-of-interest in a static photo and video. The results showed a promising demonstration for this computer vision technique in dealing with the irregular and contorted shapes that are regularly found in endoscope images [23]. Fig. 3 shows an output of the detection reported in [23].

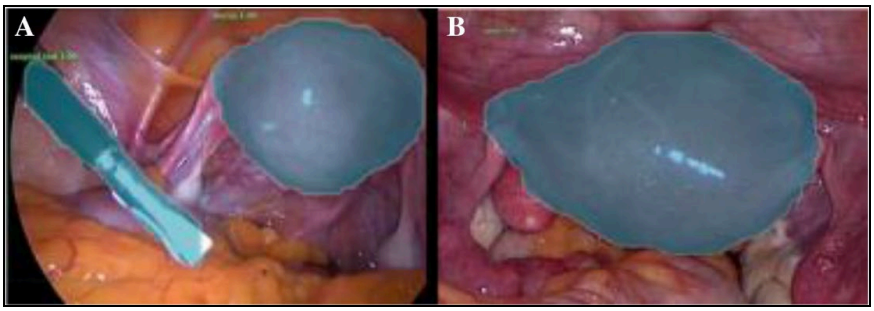

Fig. 3 - Example of an output of the Mask-RCNN-powered detection system in [23], highlighting an organ and a surgical tool

2.3 Surgical Data Science

The overall theme and motivation of this research falls under the umbrella of surgical data science. In [24], surgical data science is a recent scientific discipline that emerged from the consensual opinion by the global research community, that the "increasing access to large amounts of complex data throughout the patient-care process, complemented by advances in data-science and machine learning techniques, has set the stage for a new generation of analytics that will support decision-making and quality improvement in interventional medicine." In line with this, this paper and the overall research fall within the scope of using sensors, data science, and machine learning to augment the intraoperative surgical operation and decision-making for the surgeon. We believe that artificial intelligence will have a deep, integral role to play in surgical decision-making in the future, as healthcare becomes more complex to manage by humans alone.

3. Methodology

In the development of this visual guidance system, we need a deep learning model that can perform instance segmentation. The idea of using an instance segmentation model is to generate a mask over a target shape or region-of-interest within an image, usually one with an irregular shape and boundaries. This is useful and meaningful for surgical use cases because tissues and organs are irregularly shaped, and the surgeons are trained to detect them with visual precision. Instance segmentation is the computer vision technique that is suited for this task and for the image modality in this scenario, which is endoscope images. Our chosen model is YOLACT++, the improved version of YOLACT, which is a simple, fully-convolutional model for real-time (more than 30 frames per second) instance segmentation model [25]. We tested this model on our endoscope dataset that we generated from public video of a laparoscopic cholecystectomy [26].

3.1 YOLACT Instance Segmentation Model

YOLACT, which stands for "You Only Look At the CoefficienTs", is the first competitive single-stage real-time instance segmentation method [25]. YOLACT++ is one of the few models in the world that have struck the balance between accuracy and speed performance. It achieves this by being able to generate mask prototypes as well as mask coefficients per-instance (hence the acronym) in a parallel manner, and combine both linearly to form the final masks for every instance. In this way, the model had achieved impressive results on the MS COCO dataset, in comparison with other instance segmentation deep learning models such as Mask-RCNN, PA-Net, and MS-RCNN. Overall, the model had achieved 34.1 mAP (mean average precision) on the MS COCO dataset at 33.5 fps [25]. This speed performance that is almost real-time is very crucial in laparoscopic surgery, wherein every action must be observed by the surgeon during a crucial procedure. This model has previously been applied to laparoscopy training [27]. Specifically, the original version of YOLACT was tested on a modified peg transfer exercise in a box trainer for laparoscopy training.

Table 1 - Dataset characteristics

Images (1920 by 1080 pixels)		**Labels (polygon masks)**
Training	***Validation***	***Class (only 1)***
321 images	107 images	`gallbladder`

3.2 Dataset Preparation

A video demonstration of a laparoscopic cholecystectomy [26] was used as a dataset in this experiment. The reason for this is the authors could not find medically validated and published datasets appropriate for the task of surgical palpation. A dataset of endoscopic images of gastrointestinal diseases, the Endoscopy Disease Detection Challenge 2020 dataset (EDD2020) [38], was recently released early this year for a data science challenge. It contained the following bounding-box labels: (organ 1) colon-rectal, with the associated diseases of polyp and cancer, (organ 2) esophagus, with the associated diseases of Barrett's syndrome, dysplasia, and cancer, and (organ 3) stomach and duodenum, with the associated diseases of pyloric inflammation, dysplasia, and cancer. But this dataset does not contain mask labels of actual organs, only bounding-box labels of the region where the diseases in specific organs are localized. The requirement for our experiment is a dataset of endoscope images of organs that have mask labels, potentially organs that are usually subject to surgical palpations. In line with this, we have selected the gall bladder as it is prone to lump formation that can be palpated. We downloaded the video from [26] and extracted the frames from it, and annotated the gall bladder in each frame. We listened to the voice over of the surgeon who was demonstrating the surgical procedure, and identified the gall bladder that was being operated on in the video. We believe this to be an adequate process for generating this specific dataset for our purposes in this paper. Table 1 describes our dataset. Fig. 4 shows an example of the annotated images of the gall bladder in our custom endoscope image dataset. These images belong to the training set of our custom dataset.

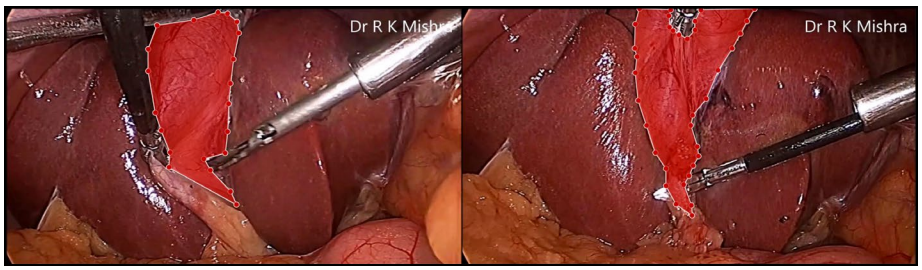

Fig. 4 - Example of the ground truth mask label of gall bladder in our custom dataset, which is extracted from [27]

3.3 Model Training

The algorithm YOLACT++, which was the improved version of the original YOLACT, was trained on a Nvidia GTX 2060 6GB VRAM GPU, with an image size of 550 pixels, a batch size of 4, and 160k iterations. The training lasted for a total of 36 hours.

3.4 Computer-generated Palpation Path Guides

The palpation path guides are inspired by the physical markers as depicted in Figure 2.c. A particular step that takes place in laparoscopic palpation is when the palpation sensor has to brush along the tissue so that it covers an

adequate range of area over which the lump is suspected to be located. In the experiment in [1], the physical markers are placed on a range of area on the silicon tissue model where there is no lump and where there is lump. This is intended to observe the change in the accelerometer signal that would indicate the change in the altitude of the tissue model. The same principle is also used in contact-based palpation sensors such as in [14].

With this in mind, OpenCV was used to generate the palpation path guides over the detected gall bladder [32]. Instead of an array of marks that the end-effectors have to prod onto, the computer-generated palpation path guide in this experiment is drawn as a table, with the inner boxes being the space onto which the end-effectors will prod, to perform the palpation described in [1]. This version of palpation path guide is developed with OpenCV's function called selectROI, which follows the part of the image that has been selected by a user or by a program [32]. In this scenario, once YOLACT++ has localized the target organ, the selectROI function follows it and draws the palpation path guide inside the mask generated by YOLACT++.

4. Results and Discussion

Example results can be viewed on our project website at https://kerwincaballas.github.io/lap-palpation. Table 2 shows the performance of the YOLACT++ model after training. It achieved a bounding-box detection accuracy of 92.17 AP and mask detection accuracy of 88.37 AP on our dataset described in Table 1. The processing speed was 20.64 fps, while the video playback speed was 20.28 fps. This translates to a latency of approximately 48 ms, representing the delay between the processed video with the detections, and the input video. Fig. 5 shows the training loss attained from training the YOLACT++ model on the dataset described in Table 1. The losses plotted are class confidence, mask loss, bounding box loss, and segmentation loss. Fig. 6 shows the graph of average precision for the single-class bounding box and masks through iterations up to 160k iterations. Fig. 7 shows examples of the resulting masks of some test images. The top row shows successful masks, which have accurately identified the gall bladder in the video. The class confidence scores in successful masks have fluctuated wildly between 0.60 and 1.00 on

Table 2 - YOLACT++ Model Performance After Training

Accuracy	Bounding box	92.17 AP
	Mask	88.37 AP
Speed Performance	Processing	20.64 fps
	Video playback	20.28 fps
Video Latency	~48 ms	

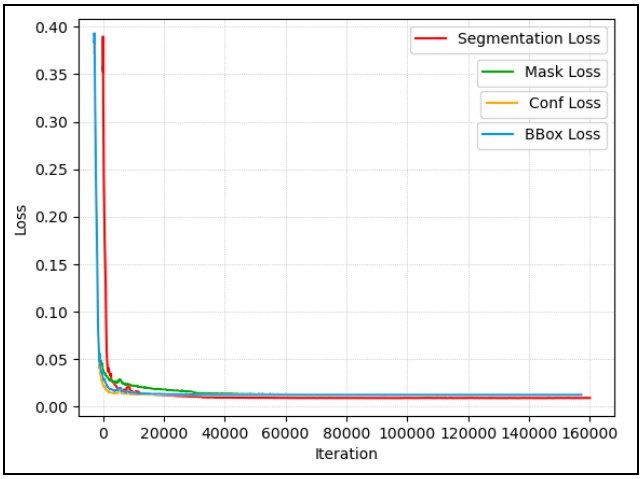

Fig. 5 - Training loss curves (segmentation loss, mask loss, class confidence loss, and bounding box loss)

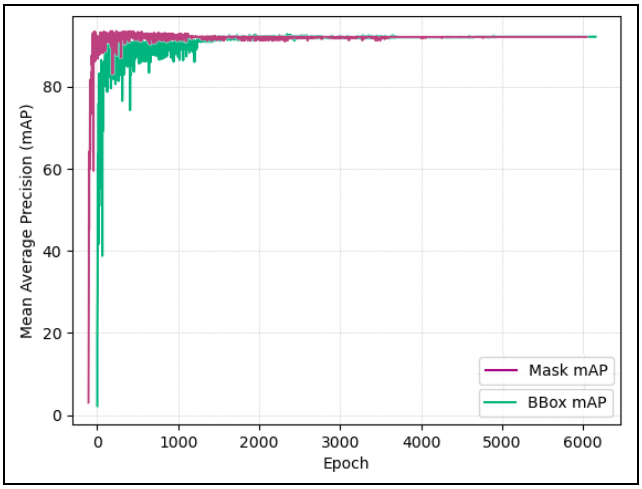

Fig. 6 - Average precision for bounding-box detection (green) and mask detection (maroon) over epoch

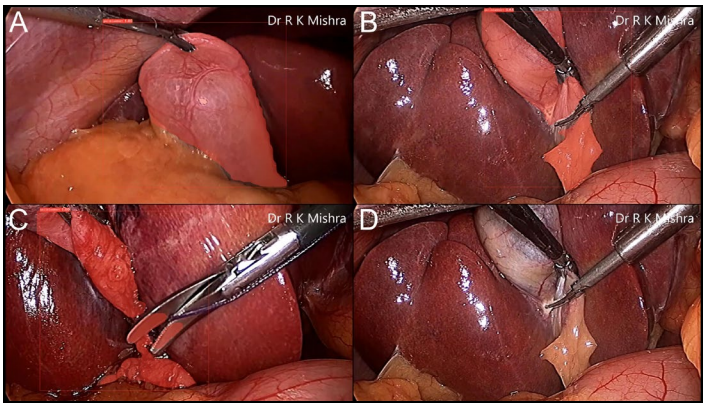

Fig. 7 - Examples of output masks. Top-row: successful cases. Bottom-row: failure cases

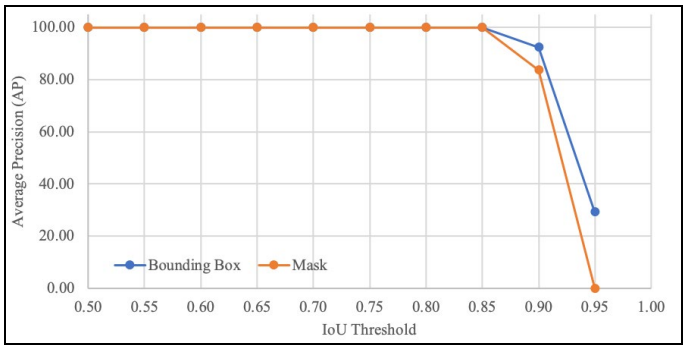

Fig. 8 - Average precision of the bounding-box (blue) and mask (orange) detections at certain IoU thresholds

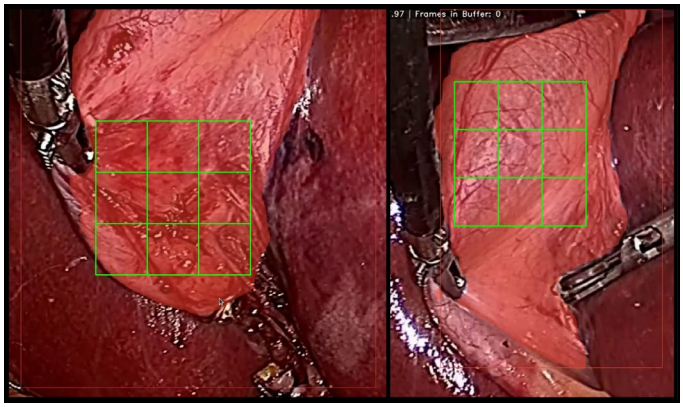

Fig. 9 - Examples of the output palpation path guides

both test images and video. The masks are accurate but not always perfect. The bottom row shows failure cases wherein the mask has included regions that are not gall bladder (like including the end-effector in C), or the mask has not totally covered the entire gall bladder in the frame, or the mask has not appeared at all (as in D). Fig. 8 shows the average precision at certain Intersection-over-Union (IoU) thresholds. Fig. 9 shows the current form of the palpation path guides, a green 3x3 table inside the red bounding box and red mask generated by the YOLACT++ model.

Table 3 shows a comparative analysis of the developed prototype with other works that have deep learning models for detection and classification of objects during laparoscopic surgery (bold indicates best performance). The work in [29] used the object detection system YOLO9000 on a dataset of 8,108 images of surgical tools only, while the work in [23] used the popular Mask-RCNN model to detect and classify two classes of organs (uterus and ovaries) and 1 class of surgical tool (grasper) on a dataset of 461 images with a total number of annotations of 886 instances. As seen in the table, the work in [23] delivered the highest accuracy in terms of bounding box detection, 97 mAP for uterus, and an equally impressive 86 mAP for surgical tools. It is reported in the YOLACT++ paper that the accuracy of Mask-RCNN is higher than that of YOLACT++. However, our bounding box detection accuracy is still excellent. Our work can also be considered as more practical at this stage because it is considered almost real-time. Better computing resources can surely push this towards true real-time with zero latency.

Table 3 - Comparative analysis of our system versus other works

Work	Kyungmin, et al. (2019) [29]	Zadeh, et al. (2020) [23]	Ours
Objects	7 classes of end-effectors	**2 classes of organs and 1 class of surgical tools**	1 class of organ
Model	YOLO9000	Mask-RCNN	YOLACT++
Training dataset size	**8,108 images**	461 images with 886 instances	428 images
Surgical environment	**Real**	**Real**	**Real**
Bounding box detection	84.7 mAP	**97 mAP for uterus**, 24 mAP for ovaries, and 86 mAP for surgical tools	92.17 AP
Mask detection	N/A	84.5 mAP for uterus, 29.6 mAP for ovaries, and 54.5 mAP for surgical tools	**88.37 AP**
Processing speed	**38 fps**	N/A	20.64 fps
Video playback speed	N/A	N/A	**20.28 fps**
Latency	N/A	N/A	**~54 ms**
Real-timeness	N/A	N/A	**Near real-time**

Nevertheless, we attribute the very high accuracies of our experiment with the YOLACT++ model (as shown in Table II and Fig. 8) to the limited nature of our dataset, having only one class for classification. If we had annotations

of other organs and tools, we might see a vastly different set of results. It will be considered in future iterations of this work. Regarding the palpation path guides, the size of the boxes can be adjusted based on the size of the end-effectors, to accommodate differences in the magnification settings of the laparoscope. The current form of the palpation path guides in Fig. 9 may seem intuitive to the authors, but it has not yet undergone testing and critique from medical professionals and surgeons. Currently, it can still be considered as a very early-stage user interface feature that should be tested with surgeons as end-users of this proposed system. We do envision that this visual guidance system, especially with the computer-generated palpation path guide, will be usable in other forms of contact-based laparoscopic palpation, wherein the same principle of targeting areas on an organ's surface is followed.

Insofar as instance segmentation is concerned, YOLACT++ shows promise in being an effective computer vision model for use in various functions during laparoscopic surgery. The use of computer vision techniques, such as instance segmentation for this study, are steps towards the realization of image-guided surgery, with artificial intelligence playing a fundamental role [30-31]. Computer vision is one of the most useful technology that can vastly improve surgery in the future. The applications of computer vision are certainly broadening in scopes, due to the increasing access of visual surgical data especially with the proliferation of minimally invasive surgical techniques. Intraoperative video analysis is one of the ways in which computer vision is expected provide a lot of value in surgery, wherein use cases include recognition of the different phases of surgery as well as detection and classification of organs and tools, that can be useful in ensuring a safer operating room for the patient [31].

5. Conclusion

A visual guidance system for use during intraoperative laparoscopic surgery is presented. The proposed system is designed to be a part of a larger motion-based laparoscopic palpation system that is meant for allowing laparoscopic surgeons to perform palpation during minimally invasive surgical operations. In line with this, the visual guidance subsystem, built with deep learning-powered computer vision, aims to contribute a layer of visual guidance that assists the surgeon in targeting the end-effector for prodding and thus executing the motion-based palpation technique. The implementation of the YOLACT++ model, an effective instance segmentation visual algorithm, achieves effective performance in terms of highlighting the irregularly shaped target organ in video, achieving about 92.17 AP on bounding box detection and 88.37 AP on mask detection of the gall bladder during a laparoscopic cholecystectomy. The palpation path guides prototype is developed using an open-source computer vision library, although more iteration, testing, and critique by real surgeons and medical professionals, is required to fully support its utility and effectiveness. Nevertheless, the proposed subsystem paves the way for further progress towards image-guided surgery, using artificial intelligence to vastly improve the current state of intraoperative laparoscopic surgery. Future updates to our overall prototype will be posted on our project website at https://kerwincaballas.github.io/lap-palpation.

Compliance with Ethical Standards

Disclosures: All authors have no conflict of interest or financial ties to disclose. The sensitive dataset used in this study was extracted from a video that was published on YouTube, a public video-hosting platform. Identity of the patient is not known by the authors and is left anonymous by the original publisher and rightful owner of the said video. No license, copyright, or any kind of intellectual property, as well as individual privacy were compromised in this study.

Acknowledgement

This research is supported through the Philippine Department of Science and Technology, Science Education Institute's Engineering Research and Development for Technology (DOST-ERDT) Scholarship and Research Grant. We also acknowledge Dr. R. K. Mishra of the World Laparoscopy Hospital, India, for his publicly available video demonstration of laparoscopic cholecystectomy.

References

[1] Caballas, K., et al. (2020). Development of a novel laparoscopic palpation system using a wearable motion-sensing armband, 11th Asian Pacific Conference on Medical and Biological Engineering (APCMBE 2020), Okayama, Japan, paper #063.

[2] Bolingot, H. J. M., Abrajano, G., Libatique, N. J., Reyes, D. A., Tangonan, G. (2017). Simulated Laparoscopic Training and Measurement Systems Based on a Low-Cost sEMG and IMU Armband, 39th Annual International Conference of the IEEE Engineering in Medicine and Biology Society (EMBC'17), Jeju Island, South Korea.

[3] Salud, I., Bolingot, H. J., Macaraig, L. C., Libatique, N., Tangonan, G. (2020). Surface-Based Electromyography Gesture Profiling of Laparoscopic Tools using a Wearable Sensor, 11th Asian Pacific Conference on Medical and Biological Engineering (APCMBE 2020), Okayama, Japan.

[4] Encyclopedia Britannica. Palpation. Available: https://www.britannica.com/science/palpation.

[5] Puangmali, P., Liu, H., Seneviratne, L. D., Dasgupta, P., Althoefer, K. (2012). Miniature 3-Axis Distal Force Sensor for Minimally Invasive Surgical Palpation. IEEE/ASME Trans. Mechatron, 4, 646-656.
[6] Gwilliam, J., Pezzementi, Z., Jantho, E., Okamura, A., Hsiao, S. (2010). Human vs. robotic tactile sensing: Detecting lumps in soft tissue. 2010 IEEE Haptics Symposium, 21-28.
[7] Karadeniz-Bilgili, M. Y., Braga, L., Birchard, K. R., Gerber, D., Firat, Z., Woosley, J. T., Shrestha, R., Semelka, R. C. (2006). Hepatocellular carcinoma missed on gadolinium enhanced MR imaging, discovered in liver explants: retrospective evaluation. Journal of Magnetic Resonance Imaging, 2, 210-215.
[8] Seçil, M., Obuz, F., Altay, C., Gencel, O., Igˇci, E., Sagˇol, O., Dicle, O. (2008). The role of dynamic subtraction MRI in detection of hepatocellular carcinoma. Diagnostic and Interventional Radiology, 4, 200-204.
[9] Ahmed, H. U., Kirkham, A., Arya, M., Illing, R., Freeman, A., Allen, C., Emberton, M. (2009). Is it time to consider a role for MRI before prostate biopsy?. Nature Reviews Clinical Oncology, 4, 197-206
[10] Ohtsuka, T., Furuse, A., Kohno, T., Nakajima, J., Yagyu, K., Omata, S. (1995). Application of a new tactile sensor to thoracoscopic surgery: experimental and clinical study. The Annals of Thoracic Surgery, 60, 610-614.
[11] Brauck, K., Zenge, M., Stock, F., Mark, L., Vogt, F., Barkhausen, J. (2006). Multi-contrast whole-body 2-D axial MR imaging during continuous table movement for tumor staging. Proc. Intl. Soc. Mag. Reson. Med., 1793.
[12] Puangmali, P., Althoefer, K., Seneviratne, D., Murphy, D., Dasgupta, P. (2008). State-of-the-art in force and tactile sensing for minimally invasive surgery. IEEE Sensors Journal, 4, 371-381.
[13] Schostek, S., Schurr, M. O., Buess, G. F. (2009). Review on aspects of artificial tactile feedback in laparoscopic surgery. Medical Engineering & Physics, 8, 887-898.
[14] Trejos, A. L., Patel, R. V., Naish, M. D. (2010). Force sensing and its application in minimally invasive surgery: a survey. Proceedings of the Institution of Mechanical Engineers, Part C: Journal of Mechanical Engineering Science, 7, 1435-1454.
[15] Buess, G. F., Schurr, M. O., Fischer, S. C. (2000). Robotics and allied technologies in endoscopic surgery. Archives of Surgery, 135, 229-235.
[16] Peirs, J., Clijnen, J., Reynaerts, D., van Brussel, H., Herijgers, P., Corteville, B., Boone, S. (2004). A micro optical force sensor for force feedback during minimally invasive robotic surgery. Sensors and Actuators A: Physical, 115, 447-455.
[17] Seibold, U., Kuebler, B., Hirzinger, G. (2005). Prototype of instrument for minimally invasive surgery with 6-axis force sensing capability. Proceedings of the 2005 IEEE International Conference on Robotics and Automation, 496-501.
[18] Rebello, K. J. (2004). Proceedings of the IEEE, 1, 43-55.
[19] Valdastri, P., Harada, K., Menciassi, A., Beccai, L., Stefanini, C., Fujie, M., Dario, P. (2006). Integration of a miniaturised triaxial force sensor in a minimally invasive surgical tool. IEEE Transactions on Biomedical Engineering, 11, 2397-2400.
[20] Baumhauer, M., Feuerstein, M., Meinzer, H. P., Rassweiler, J. (2008). Navigation in Endoscopic Soft Tissue Surgery: Perspectives and Limitations. Journal of Endourology, 4, 751-766.
[21] Mirota, D. J., Ishii, M., Hager, G. D. (2011). Vision-Based Navigation in Image-Guided Interventions. Annual Review of Biomedical Engineering, 1, 297-319.
[22] Mountney, P., Stoyanov, D., Yang, G. Z. (2010). Three-Dimensional Tissue Deformation Recovery and Tracking. IEEE Signal Processing Magazine, 4, 14-24.
[23] Zadeh, S. M., et al. (2020). SurgAI: deep learning for computerized laparoscopic image understanding in gynaecology. Surgical Endoscopy, 12, 5377-5383.
[24] Maier-Hein, L., et al. (2017). Surgical data science for next-generation interventions. Nature Biomedical Engineering, 9, 691-696.
[25] Bolya, D., Zhou, C., Xiao, F., Lee, Y. J. (2020). YOLACT++: Better Real-time Instance Segmentation. IEEE Transactions on Pattern Analysis and Machine Intelligence, 1-1.
[26] Mishra, R. K. (2014). Laparoscopic surgery for gall stone. Available: https://www.youtube.com/watch?v=rt3SGf7YJT8.
[27] Bolingot, H. J. & Shibata, T. (2019). Beyond Tool Motion Analysis: Exploring Potential Innovations for Augmenting Laparoscopic Surgery Skill Analysis and Training. IEEE Engineering in Medicine and Biology International Student Conference 2019, Magdeburg, Germany: Book of Proceedings, 40.
[28] Ali, S., et al. (2020). Endoscopy Disease Detection and Segmentation (EDD2020). Available: https://ieee-dataport.org/competitions/endoscopy-disease-detection-and-segmentation-edd2020.
[29] Kyungmin, J., et al. (2019). Robust Real-Time Detection of Laparoscopic Instruments in Robot Surgery Using Convolutional Neural Networks with Motion Vector Prediction. Applied Sciences, 14, 2865.
[30] Loftus, T. J., et al. (2020). Artificial Intelligence and Surgical Decision-making. JAMA Surgery, 2, 148.
[31] Hashimoto, D. A., Ward, T. M., Meireles, O. R. (2020). The Role of Artificial Intelligence in Surgery. Advances in Surgery, 54, 89-101.
[32] Uddin, M (2020). misbah4064/object_tracking. Available: https://github.com/misbah4064/object_tracking.